*J Neurophysiol* 110: 577–586, 2013.
First published April 17, 2013; doi:10.1152/jn.00164.2013.

# Noise-induced cochlear neuropathy is selective for fibers with low spontaneous rates

**Adam C. Furman,[2,4] Sharon G. Kujawa,[1,3,4] and M. Charles Liberman[1,2,4]**

[1]*Department of Otology and Laryngology, Harvard Medical School, Boston, Massachusetts;* [2]*Eaton-Peabody Laboratory, Massachusetts Eye and Ear Infirmary, Boston, Massachusetts;* [3]*Department of Audiology, Massachusetts Eye and Ear Infirmary, Boston, Massachusetts; and* [4]*Harvard Program in Speech and Hearing Bioscience and Technology, Boston, Massachusetts*

Submitted 5 March 2013; accepted in final form 10 April 2013

**Furman AC, Kujawa SG, Liberman MC.** Noise-induced cochlear neuropathy is selective for fibers with low spontaneous rates. *J Neurophysiol* 110: 577–586, 2013. First published April 17, 2013; doi:10.1152/jn.00164.2013.—Acoustic overexposure can cause a permanent loss of auditory nerve fibers without destroying cochlear sensory cells, despite complete recovery of cochlear thresholds (Kujawa and Liberman 2009), as measured by gross neural potentials such as the auditory brainstem response (ABR). To address this nominal paradox, we recorded responses from single auditory nerve fibers in guinea pigs exposed to this type of neuropathic noise (4- to 8-kHz octave band at 106 dB SPL for 2 h). Two weeks postexposure, ABR thresholds had recovered to normal, while suprathreshold ABR amplitudes were reduced. Both thresholds and amplitudes of distortion-product otoacoustic emissions fully recovered, suggesting recovery of hair cell function. Loss of up to 30% of auditory-nerve synapses on inner hair cells was confirmed by confocal analysis of the cochlear sensory epithelium immunostained for pre- and postsynaptic markers. In single fiber recordings, at 2 wk postexposure, frequency tuning, dynamic range, postonset adaptation, first-spike latency and its variance, and other basic properties of auditory nerve response were all completely normal in the remaining fibers. The only physiological abnormality was a change in population statistics suggesting a selective loss of fibers with low- and medium-spontaneous rates. Selective loss of these high-threshold fibers would explain how ABR thresholds can recover despite such significant noise-induced neuropathy. A selective loss of high-threshold fibers may contribute to the problems of hearing in noisy environments that characterize the aging auditory system.

excitotoxicity; noise-induced hearing loss; auditory nerve

AUDITORY NERVE (AN) fibers transmit signals from cochlear inner hair cells (IHCs) to their brainstem targets in the cochlear nucleus. Each AN fiber receives signals from a single IHC via a single ribbon synapse (Liberman 1980; Spoendlin 1969), but each hair cell is contacted by 10–30 AN fibers depending on cochlear location and species (Bohne et al. 1982; Liberman et al. 1990; Stamataki et al. 2006). This multiple innervation is important in auditory processing, because the AN fibers contacting a single hair cell differ in spontaneous discharge rate (SR) and threshold to acoustic stimulation (Liberman 1978). The SR distribution recorded among AN fibers is fundamentally bimodal, and the low-SR (<20 sp/s) group has higher thresholds than the high-SR (>20 sp/s) group (Liberman 1978). In addition to increasing the dynamic range of the auditory periphery, the high-threshold, low-SR fibers are important for hearing in a noisy environment, by virtue of their resistance to masking by continuous background noise (Costalupes et al. 1984).

Recent work in both mouse (Kujawa and Liberman 2009) and guinea pig (Lin et al. 2011) has shown that acoustic overexposures causing reversible threshold elevations can lead to irreversible degeneration of AN fibers. The loss of hair cell synapses and AN peripheral terminals is rapid (within hours postexposure), while the loss of the AN cell bodies in the spiral ganglion is slow (months to years). The idea that cochlear neural degeneration could be a primary event, rather than only occurring secondarily to the loss of hair cells, was surprising but not paradoxical. The idea that roughly 40% of the AN cochlear synapses could be permanently destroyed without a permanent elevation of the thresholds for the auditory brainstem response, which reflects the summed activity of the AN fibers in its first wave (Melcher et al. 1996), could be explained by hypothesizing that the neural loss was selective for the subgroup of AN fibers with low SRs and high thresholds. This hypothesis was supported by the observed reduction in auditory brainstem response (ABR) wave 1 amplitudes at suprathreshold stimulus levels (Kujawa and Liberman 2009).

The aim of the present study was to directly test this hypothesis by recording from populations of AN fibers animals exposed to a noise designed to produce cochlear neuropathy without permanent threshold shift. We chose the guinea pig, because its larger size makes it easier to record from large populations of single AN fibers. We found that the surviving fibers in these noise-exposed ears show responses that are normal in all respects except that the proportion of fibers with low SR is significantly smaller than in unexposed ears. We speculate that this selective low-SR neuropathy contributes to the difficulties of hearing in noisy environments that constitute the classic audiometric deficit in the aging ear.

## MATERIALS AND METHODS

*Animals and groups.* Female, albino guinea pigs (Hartley strain) were used in all experiments. All procedures were approved by the Institutional Animal Care and Use Committee at the Massachusetts Eye and Ear Infirmary. Animals entered the protocol at 1 mo of age (~250 g), when cochlear thresholds were tested by measurement of ABRs and distortion product otoacoustic emissions (DPOAEs). At least 2 days after recovery from the sedation required for this test, nine animals were sound exposed (4- to 8-kHz octave-band noise at 106 dB SPL for 2 h) and allowed to recover. The other 14 animals served as nonexposed controls. Control and exposed animals were caged to-

Address for reprint requests and other correspondence: M. C. Liberman, Eaton-Peabody Laboratory, Massachusetts Eye and Ear Infirmary, 243 Charles St., Boston, MA 02114-3096 (e-mail: Charles_Liberman@meei.harvard.edu).

gether throughout the experimental protocol. Two weeks after exposure, ABRs and DPOAEs were remeasured, and single-fiber data were collected from the cochlear nerve. At the end of the terminal experiment, the cochleas were extracted, and tissue was proceessed for confocal microscopy.

*ABR and DPOAE measures.* ABR and DPOAE responses were measured in an acoustically and electrically shielded chamber, heated to 30°C. Animals were anesthetized with a mixture of pentobarbital (25 mg/kg ip), fentanyl (0.15 mg/kg im), and droperidol (7.5 mg/kg im). Acoustic stimuli were delivered via a custom acoustic assembly comprising two earphones to deliver sound and an electret condenser microphone (Knowles FG-23329-P07) coupled to a probe tube to measure sound pressure level. For ABRs, needle electrodes were placed near the ear canal at its caudoventral aspect, the vertex of the skull, and a ground at the lower back. Stimuli were 4-ms tone pips, with a 0.5-ms rise/fall delivered at 30/s. Stimulus polarity was alternated to allow removal of microphonic potentials. Responses were averaged to 512 tone-pip pairs. Tone-pip frequency was varied from 2.8 to 45.2 kHz in half-octave steps, and stimulus level was varied from 10 to 80 dB SPL in 5-dB steps. ABR threshold was measured, by visual inspection of stacked waveforms, as the lowest SPL at which any ABR wave was visible, which was typically 5 dB less than the lowest level at which the peak-to-peak amplitude of the waveform emerged from the noise floor. DPOAEs were measured in response to two pure tones (f2 and f1 with f2/f1 = 1.2 and with a 10-dB level difference such that f1 = f2 + 10 dB). DPOAE response was measured as the amplitude of the 2f1-f2 peak extracted from a Fourier transform of the averaged probe tube microphone response. Both waveform and spectral averaging were used. DPOAE threshold was defined as the interpolated primary level (of f2) required to produce a DPOAE of 0 dB SPL.

*Single-fiber recordings.* Animals were anesthetized with a combination of urethane (900 mg/kg ip), fentanyl (0.15 mg/kg im), and droperidol (7.5 mg/kg im). Once a surgical plane of anesthesia was reached, ear canals were severed, and muscle tissue was removed from the bulla and the back of the skull. The bulla was opened, and a silver wire was placed close to the round window to monitor the compound action potential (CAP). The occipital bone was opened, the dura was resected, and the cerebellar lobes on one side were aspirated to expose the cochlear nucleus, which, when displaced medially and rostrally, revealed the auditory nerve trunk as it exits the internal auditory meatus. CAPs evoked by tone pips were monitored regularly, and the experiment was terminated if thresholds shifted by >10 dB. Single-fiber responses were recorded using glass micropipettes, filled with 2 M KCl, with impedances between 10 and 30 MΩ. Electrodes were advanced remotely, while presenting a broadband noise burst (70–80 dB SPL) as a search stimulus. Spikes were amplified using a low-noise, battery-powered amplifier (Ithaco Model 1201), and spike times were digitized with custom hardware and passed to the computer for analysis. Once a neuron was isolated, the SR was measured over a 30-s sample. Acoustic stimuli were always 50-ms tone bursts with a 2.5-ms rise-fall time, presented at 10/s. The tuning curves were measured with an algorithm designed to track the isorate contour (10 spikes/s > SR). To analyze postonset adaptation, poststimulus-time histograms were recorded in response to 200 tone-burst presentations at 30 dB above threshold at the characteristic frequency (CF). To assess dynamic range, rate vs. level functions were recorded using tone bursts at CF over a range of stimulus levels (0–80 dB SPL, 50 presentations per level, presented in random level order). Rate-level functions were fit using a model published previously (Taberner and Liberman 2005). Dynamic range was defined as the difference in stimulus SPL required to drive the neurons from 10% to 90% of the maximum discharge rate.

*Histological preparation.* At the end of the single-fiber experiment, animals were perfused intracardially with 4% paraformaldehyde. After perfusion, cochleas were removed, the round and oval windows were opened, and cochleas were postfixed: either overnight at 4°C, or for 1 h at room temperature if anti-GluA2 was one of the immunostains. Cochleae were then decalcified for 3 wk in EDTA (120 mM, pH 7.0) at room temperature. The organ of Corti was then microdissected into 11 pieces and immunostained. When quantitative data were to be extracted, cochleas were processed in pairs, with control and exposed ears treated with the same solutions on the same days. Tissue was permeabilized in 30% sucrose for 20 min, blocked for 1 h in 5% NHS with 1% Triton, then incubated overnight at 37°C in primary antibodies. Primary antibodies included mouse anti-CtBP2 (1:50, BD Transduction Labs, #612044), goat anti-Na/K ATPase (1:100, Santa Cruz, #sc-16052), rabbit anti-myosinVIIa (1:100, Proteus BioSciences, #25-6790), and mouse (IgG2a) anti-GluA2 (1:1,000, Millipore, #MAB397). Tissue was rinsed in PBS and then incubated for 1 h at 37°C in a two-step process of secondary antibody linkage: step 1: biotinylated donkey anti-mouse (1:200, Jackson ImmunoResearch, #7115-065-150), AlexaFluor488 chicken anti-goat (1:1,000, Invitrogen, #A21467), and donkey anti-rabbit-AF647 (1:200, Invitrogen, #A31573); step 2: streptavidin-conjugated AlexaFluor568 (1:1,000, Invitrogen, #S11226), AlexaFluor488 goat anti-chicken (1:1,000, Invitrogen, #A11039), and donkey anti-rabbit-AF647 (1:200, Invitrogen, #A31573).

*Microscopy and image analysis.* A cochlear frequency map for each case was produced using a custom plug-in to ImageJ (http://www.masseyeandear.org/research/ent/eaton-peabody/epl-histology-resources/) with which the user traces the inner spiral bundle in each dissected piece, and the plug-in measures position along the spiral and applies a physiological place-frequency map (Tsuji and Liberman 1997) to overlay frequencies onto the montaged cochlear pieces. With this "road map" as a guide, IHC synaptic zones were imaged in each case at eight log-spaced frequency locations (0.5, 1, 2, 4, 8, 16, 32, and 45 kHz) on a Leica SP2. Confocal z-stacks (0.25-mm vertical spacing) were acquired with a ×100 oil-immersion objective (N.A. 1.4) and ×2 digital zoom. Each stack encompassed ~8 IHCs.

Stacks were analyzed offline using Amira (Visage Imaging). For each stack, presynaptic ribbons and postsynaptic glutamate receptor patches were counted, and their volumes estimated, using the "connected components" tool in Amira. This tool takes a user-specified pixel-intensity criterion and identifies all the voxel spaces within which all the pixels exceed the criterion intensity. By displaying each of these connected components as a surface contour superimposed on the maximum projection, the user can determine if the selected criterion captures the elements of interest, e.g., synaptic ribbons. For those cochleas from which three-dimensional volumes of synaptic elements were extracted, image stacks from control and noise-exposed ears were acquired with the same laser and photomultiplier gains, and the same pixel-intensity criterion was applied. The Amira output provides each element's xyz coordinates and volume. Further analysis of the Amira output was carried out in MATLAB (Mathworks) and with a custom C program that generates high-power thumbnail images of the native z-stack, each centered at the xyz positions captured in Amira (Liberman et al. 2011). These thumbnails allowed for easy identification of orphan ribbons or receptor patches.

## RESULTS

*Noise-induced neuropathy after reversible threshold shift.* In guinea pig, exposure to an octave-band noise (4–8 kHz) at 106 dB for 2 h results in an acute threshold shift of 40–50 dB, when measured within 12–24 h postexposure, but these thresholds recover completely within 1–2 wk (Lin et al. 2011). Prior study showed that when cochlear function is assessed via DPOAEs, both threshold and suprathreshold responses recover completely. Since DPOAEs require only the "presynaptic" component of the cochlear sensory epithelium, i.e., an intact population of outer hair cells to create distortions in the process of mechanoelectric transduction and reverse-transduce these dis-

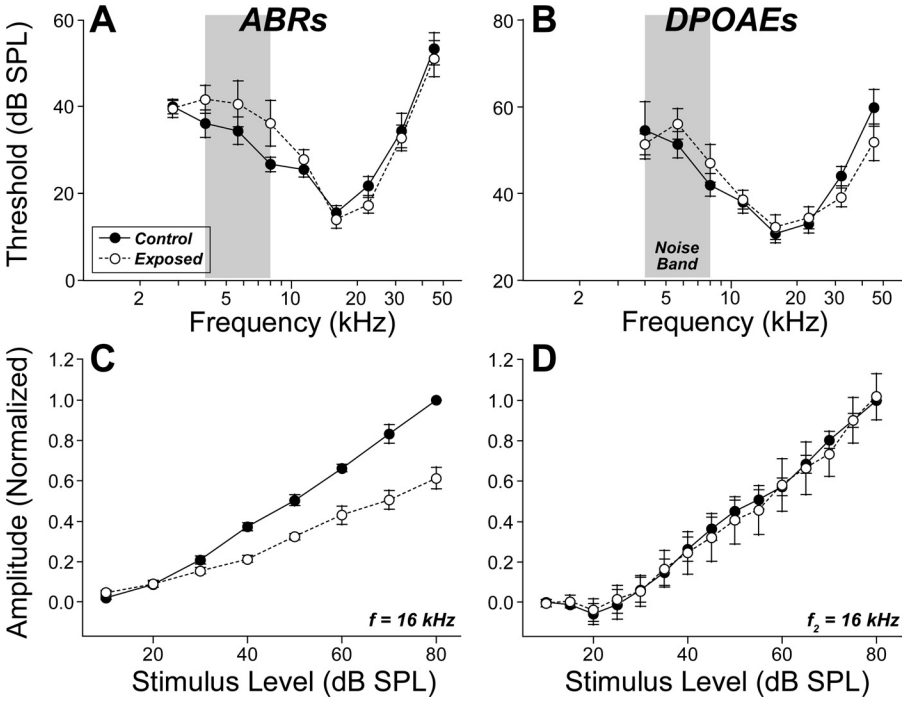


Fig. 1. After noise exposure, thresholds recover for both auditory brainstem response (ABR) and distortion product otoacoustic emissions (DPOAE), whereas suprathreshold amplitudes recover only for DPOAEs. Mean ABR (*A*) and DPOAE (*B*) thresholds (± SE) for 9 guinea pigs, before vs. 10 days after exposure to 4–8 kHz noise (gray boxes) at 106 dB SPL for 2 h. Mean amplitude-vs.-level functions (± SE) for ABR wave 1 (*C*) and DPOAEs (*D*), also measured before and 10 days after the noise exposure, for the same 9 animals shown in *A* and *B*. Amplitudes are normalized to the 80 dB SPL preexposure response for each animal. Key in *A* applies to all panels. Stimulus frequency, for tone pips and f2 primaries, was 16 kHz for *C* and *D*, respectively.

tortions back to mechanical motions and (ultimately) ear-canal sound pressures, the DPOAE recovery suggests full recovery of cochlear hair cell function. In contrast, the summed neural response, particularly wave 1 of the ABR constituting the summed responses of AN fibers, fails to recover at suprathreshold sound pressure levels, suggesting a partial degeneration of the AN (Kujawa and Liberman 2009).

Here, we replicated this neuropathic exposure in animals prior to recording from populations of single AN fibers. Two weeks after exposure to the 4- to 8-kHz octave band at 106 dB for 2 h, the ABR and DPOAE thresholds have recovered almost completely to the preexposure levels measured from the same ears (Fig. 1, *A* and *B*). Thresholds for the compound action potential (the summed AN response recorded from the cochlear capsule) were also similar in control and exposed ears (data not shown). Evaluation of suprathreshold responses suggested the presence of permanent neural damage: although the amplitude-vs.-level functions for the DPOAE responses recovered completely (Fig. 1*D*), the summed activity of the AN, seen as wave 1 of the ABR, showed a permanent deficit, i.e., a roughly 40% reduction in suprathreshold amplitudes (Fig. 1*C*).

The presence of primary neural degeneration (i.e., in the absence of hair cell loss) was confirmed by histological analysis of the cochleas after completion of the single-fiber studies. As schematized in Fig. 2*D*, the synapses on each inner hair cell are visualized by combining an immunolabel for the presyn-

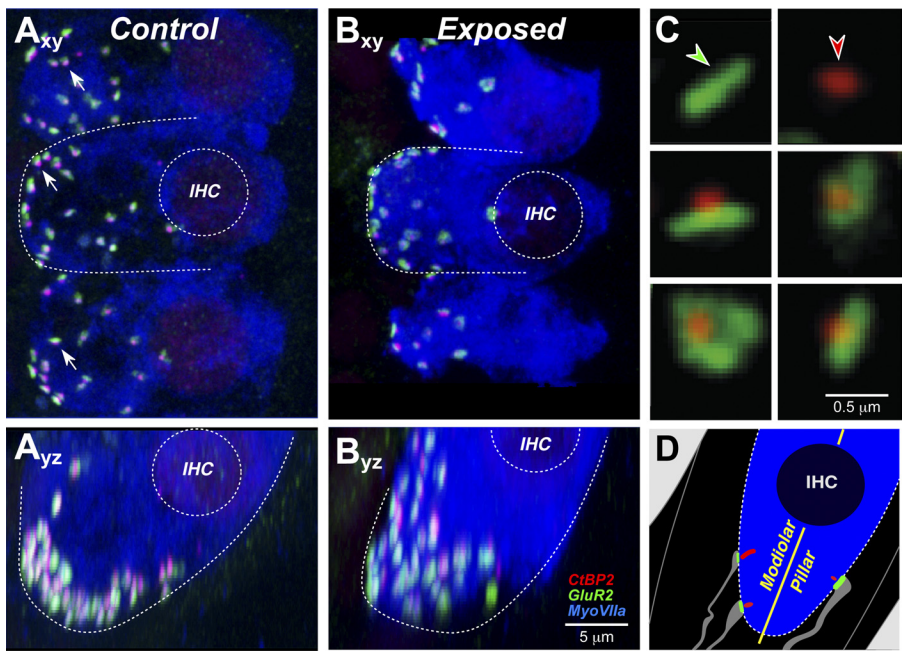


Fig. 2. Confocal analysis shows synaptic degeneration and reorganization. Cochlear tissue was triple stained for CtBP2 (red), GluA2 (green), and myosin VIIa (blue). Images from the 32-kHz region of a control (*A*) and an exposed ear (*B*) show maximum projections from "surface" views (*xy*) of 3 adjacent IHCs and side views (*yz*) of the same confocal image stacks. Outlines of IHCs and their nuclei are provided for reference. Arrows point to cochlear nerve synapses, i.e., paired CtBP2- and GluA2-positive puncta. Scale bar in B also applies to *A*. *C*: to quantify the pairing of ribbons and glutamate-receptor patches, each image stack was redisplayed to produce high-power projections of the voxel space within 1 mm of each CtBP2-positive puncta. These miniature reprojections were displayed as a thumbnail array, which allowed identification of unpaired receptor patches (green arrow) or ribbons (red arrow). *D*: schematic of the IHC base showing 3 of its 10–20 cochlear nerve synapses and the longitudinal axis dividing the modiolar and pillar sides of the IHC. Schema colors mirror the immunostains in the 3 confocal channels; cochlear nerve terminals are shown in gray.

aptic ribbon within the hair cell (anti-CtBP2) and another for the postsynaptic glutamate receptor patch on the AN terminal (anti-GluA2). In a normal ear (Fig. 2*A*), synapses appear as pairs of puncta: a CtBP2-positive patch and a closely apposed GluA2-positive patch. The synapses are distributed around the basolateral membrane of the inner hair cell in the subnuclear zone, as clearly seen in the z-stack "side view" shown in Fig. 2*Ayz*. In the exposed ear (Fig. 2*B*), the number of synapses is reduced (Fig. 2*Bxy*) and the distribution around the basolateral membrane appears less tightly clustered (Fig. 2*Byz*). High-power thumbnails of the synapses (Fig. 2*C*) reveal that in the exposed ear, some of the ribbons are no longer paired with postsynaptic receptor patches.

Quantitative synaptic analysis from a large sample of exposed and control cochleas (Fig. 3*A*) shows a reduction in synaptic counts for all cochlear regions in the basal half of the cochlea (frequencies $\geq$ 4 kHz). The intergroup differences were highly significant ($P \ll 0.01$ by 2-way ANOVA). The normalized data (Fig. 3*B*) show that the fractional synaptic reduction increases steadily towards the base with a maximum loss of close to 30% at 32 kHz. The high-power analysis (Fig. 3*C*) reveals that *1*) in both normal and noise-exposed ears, more than 95% of all ribbons are paired with glutamate receptor patches (i.e., likely represent true synapses), and *2*) there is a modest increase in the number of "orphan" ribbons (i.e., without paired receptor patches) in the basal turn of the exposed ears.

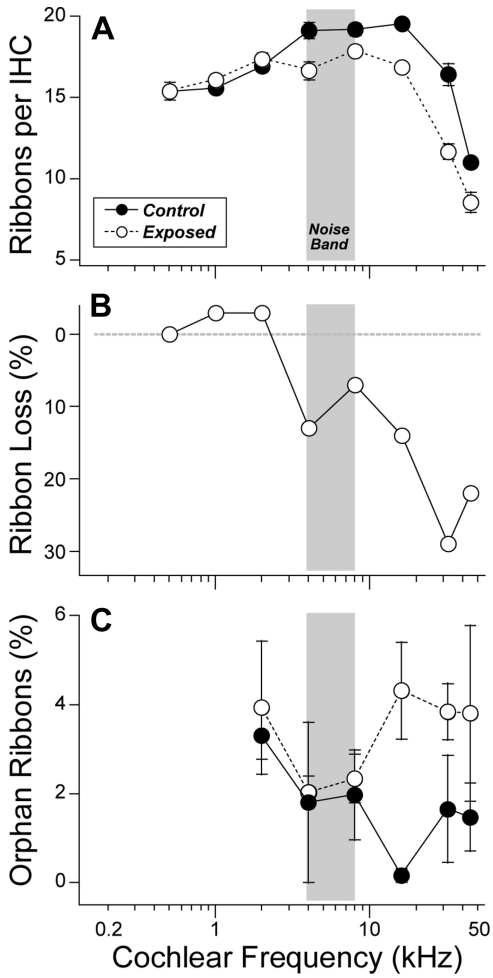


Fig. 3. IHC synaptic counts are reduced by the noise exposure. *A*: mean counts of IHC synaptic ribbons (± SE) in control ($n$ = 5) vs. noise-exposed ($n$ = 14) ears. In each cochlear region, in each ear, two adjacent z-stacks were acquired, each including 75 $\mu$m of cochlear length (encompassing 7–9 adjacent IHCs). *B*: ribbon counts from *A* expressed as % decrease from controls. *C*: orphan ribbons, i.e., those without a juxtaposed glutamate-receptor patch, are rare in both control ($n$ = 2) and exposed ($n$ = 6) ears, although the prevalence increases postexposure in the high-frequency region. Data are group means (± SE). Postexposure data in all panels were acquired 2 wk after noise; controls were unexposed and age matched. Gray boxes indicate the frequencies of the octave-band noise exposure.

*Responses of single AN fibers after reversible threshold shift.* The frequency tuning of AN fibers is dominated by cochlear mechanics, which, in turn, is shaped, at low sound pressure levels, by the cochlear amplification provided by the electromechanical motors of the outer hair cell (Cheatham et al. 2004). Given the complete postexposure recovery of DPOAEs (Fig. 3), and the implied recovery of outer hair cell function, no postrecovery changes in AN frequency tuning were expected in the exposed ears. Indeed, frequency tuning curves of single ANs measured in exposed ears were similar to those in unexposed controls, as illustrated in Fig. 4*A*, in which representative pre- and postexposure curves are paired by matching the CF, which also pinpoints the location of each fiber's hair cell synapse along the cochlear spiral (Liberman 1982a).

One commonly used metric of AN tuning is the "quality factor," or Q, defined as the CF divided by the bandwidth, typically measured 10 dB above the minimum threshold (Kiang et al. 1965). As shown by comparing the data in Figs. 4, *B* and *C*, the distributions of $Q_{10}$ in exposed vs. unexposed groups were not significantly different: after separating by SR [low-SR <1 sp/s, high-SR >20 sp/sec, with medium-SR in between (Tsuji and Liberman 1997)] and by CF (low CF $\leq$4 kHz; high CF >4 kHz), none of the exposed vs. unexposed differences was significant by the Kolmogorov-Smirnov test ($P > 0.05$).

Given the near-complete postexposure recovery of ABR thresholds (Fig. 1*A*), we expected near-complete recovery of AN thresholds, certainly for the low-threshold, fiber population with high SRs. Indeed, the high-SR fibers in the exposed ears (Fig. 4*D*) showed mean thresholds similar to those seen in high-SR fibers in the unexposed ear (Fig. 4*D*): the two groups were statistically indistinguishable ($P > 0.01$ by Kolmogorov-Smirnov). The mean thresholds of the medium-SR groups were slightly higher in the postexposure group for CFs >4 kHz. However, the differences were not significant ($P > 0.05$ by Kolmogorov-Smirnov). The effect of the exposure on low-SR thresholds is more difficult to gauge, because the prevalence of low-SR fibers in the postexposure sample appears to be significantly reduced, especially for CF regions at and above the exposure band (Fig. 4*C*).

A disproportionate loss of low-SR fibers is borne out by the statistical analysis summarized in Fig. 5: out of a total sample of 367 fibers from 14 control animals, and 382 fibers from 9 exposed animals, the proportion of fibers with SR <20 sp/s was reduced at high CF (>4 kHz), where noise-induced loss of synapses was observed (Fig. 3, *A* and *B*). For CF >4 kHz, low- and medium-SR fibers comprised 47% of the total population in control ears vs. 29% in the exposed ears, a fractional loss of 38% and a highly significant difference between the control and exposed distributions (Kolmogorov-Smirnov, $P \ll 0.01$). In contrast, in the apical half of the cochlea (CF $\leq$4 kHz),

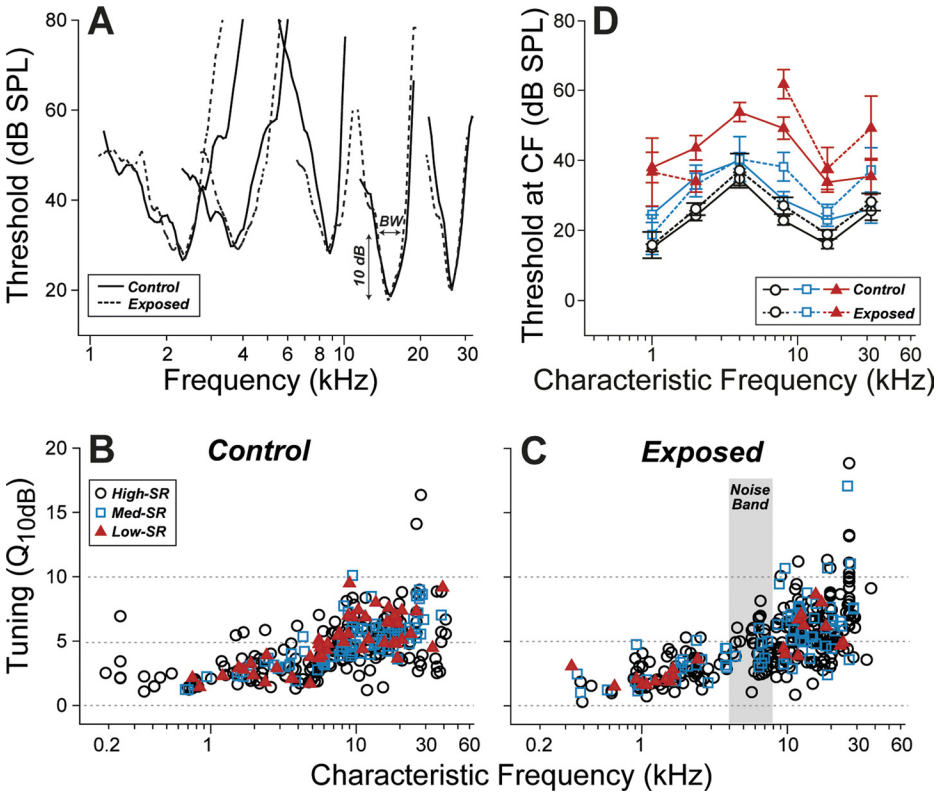


Fig. 4. Tuning and threshold of cochlear nerve fibers were unchanged by the noise exposure. *A*: tuning curves of fibers matched for characteristic frequency (CF) and spontaneous discharge rate (SR) group appear similar in control vs. noise-exposed ears. Sample threshold curves are shown here for pairs of high-SR fibers with similar CF. Sharpness of tuning ($Q_{10dB}$: the ratio between CF and bandwidth at 10 dB above minimum threshold) normally increases with increasing CF, but has little dependence on SR (*B*). $Q_{10dB}$ appears unaffected by the noise exposure. Key in *B* also applies *C*. *D*: mean thresholds at CF (± SE) for each SR group were computed by dividing the database into 6 log-spaced CF bins. SR group was defined as suggested by a prior study (Tsuji and Liberman 1997) and coded as symbol type. The single-fiber database includes 367 fibers from 14 control animals, and 382 fibers from 9 exposed animals.

where noise-exposure effects on synaptic counts were minimal (Fig. 3, *A* and *B*), the distribution of SRs postexposure was similar to that seen in unexposed controls, and the differences between distributions were not statistically significant ($P > 0.05$ by Kolmogorov-Smirnov).

To look for signs of synaptic dysfunction in remaining AN fibers of all SR groups, we evaluated several additional aspects of AN response that are shaped, at least in part, by the process of synaptic transmission.

The first of these was dynamic range. For most AN fibers, there is a relatively small range of stimulus levels between that eliciting a just detectable response (threshold) and that evoking a maximum (saturated) rate. In guinea pigs, dynamic range is typically <30 dB for high-SR fibers and can be as large as 60 dB for low-SR fibers, with little dependence on CF (Winter et al. 1990). Indeed, our rate-level functions underestimate the dynamic range of some low-SR fibers, because discharge rate is often still growing at the highest levels routinely presented (80 dB SPL: see Fig. 6 *inset*). As shown in Fig. 6, we saw no significant effect of the noise exposure on the measured dynamic ranges, and the differences between distributions, after separating by SR and CF, were not statistically significant ($P > 0.05$ by Kolmogorov-Smirnov).

The second set of postsynaptic response features evaluated was the time constants of postonset adaptation, thought to represent the depletion of different pools of synaptic vesicles (Neef et al. 2007). In response to tone bursts, the poststimulus-time histograms of AN fibers show a prominent onset response followed by a decreasing response probability that approaches a lower steady-state rate with a decay function that is well fit as the sum of two exponentials (Westerman and Smith 1984). In the normal mouse AN, those time constants average roughly 1 and 10 ms (Fig. 7, *A* and *C*). No significant changes in the time constants of postonset adaptation were observed postexposure (Fig. 7, *B* and *D*). Intergroup differences, after segregating by SR and by CF, were not significant ($P > 0.05$ by Kolmogorov-Smirnov).

The last response features we evaluated were the first-spike latency (Fig. 7, *E* and *F*) and the variance of the first-spike latency (Fig. 7, *G* and *H*). In response to tone bursts, the latency of the first spike increases with decreasing CF largely because of the slowing

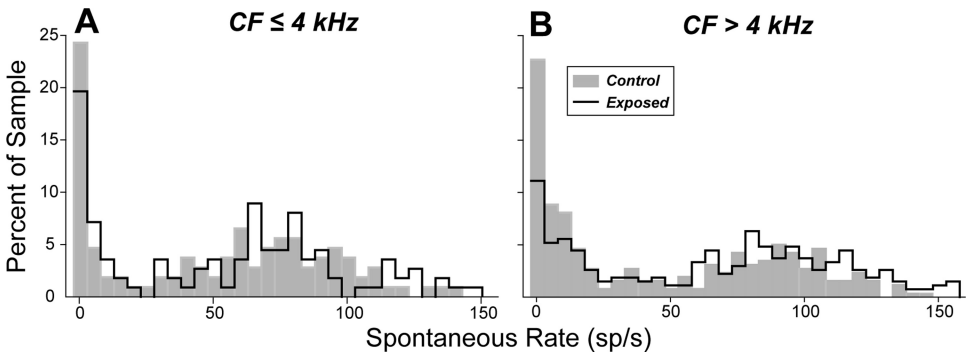


Fig. 5. Spontaneous rate distributions suggest selective loss of low-SR fibers in the high-frequency region. SR distribution plotted as percentage of total for fibers with CF ≤ 4 kHz (*A*) and with CF > 4 kHz (*B*). The fiber sample is the same as that described in the legend to Fig. 4.

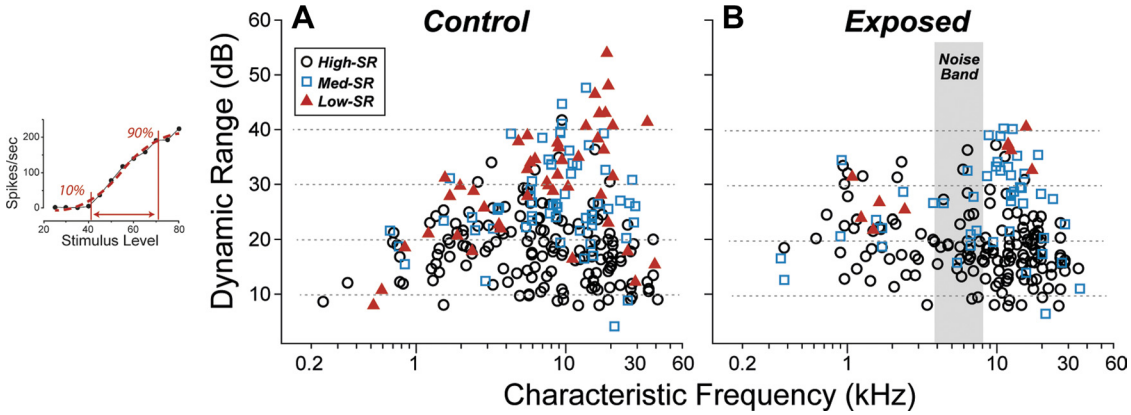


Fig. 6. Dynamic range of surviving cochlear nerve fibers was unchanged by the noise exposure. As shown in the *inset* (*left*), dynamic range is the difference, in dB, between the stimulus levels eliciting 10% and 90% of the maximum driven rate (maximum rate minus spontaneous rate). Measures are made on the model fit (red dashed line in *inset*), not the raw data (black symbols in *inset*). Key in *A* also applies to *B*. The fiber sample in *A* and *B* is the same as that described in the legend to Fig. 4. The data in the *inset* are from a low-SR fiber in a control ear.

of the cochlear traveling wave as it progresses from base to apex (Kiang et al. 1965). More relevant to synaptic processes is the variance of the first spike latency, which is greatly increased, in mice, by a mutation affecting the coupling of the synaptic ribbon to the presynaptic active zone (Buran et al. 2010). Neither the first-spike latency, nor the variance of the first-spike latency, was affected by the noise exposure. Intergroup differences, after segregating by SR and CF, were not significant ($P > 0.05$ by Kolmogorov-Smirnov).

*Modiolar/pillar gradients in hair cell synaptic morphology after reversible threshold shift.* Single-fiber labeling studies have shown that AN fibers are spatially segregated around the inner hair cell circumference according to SR group (Liberman 1982b). As schematized in Fig. 2*D*, high-SR fibers tend to contact the side of the hair cell closer to the pillar cells while the low- and medium-SR fibers tend to contact the side closer to the cochlear nerve trunk (modiolus). Furthermore, the presynaptic ribbons at low-SR synapses tend to be larger and more complex than those at high-SR synapses (Liberman et al. 1990; Merchan-Perez and Liberman 1996). This normal modiolar/pillar gradient in ribbon size, first described in cat, is visible in data from the unexposed guinea pigs in the present study, as shown in Fig. 8 for cochlear regions tuned to 2 kHz (Fig. 8, *A* and *G*), 16 kHz (Fig. 8, *C* and *H*), and 32 kHz (Fig. 8, *E* and *I*).

Given the disproportionate loss of low- and medium-SR fibers noted in the physiological analysis (Fig. 5), we might have expected a trend towards smaller ribbons on the modiolar side of the hair cell. Surprisingly, the data suggest the opposite, i.e., an increase in the ribbon size on the pillar side of the hair cell, especially in the high-CF cochlear regions (Fig. 8, *H* and *I*) where the neuropathy was most pronounced (Fig. 3, *A* and *B*), and a trend towards smaller ribbons on the modiolar side in the most apical region (Fig. 8*G*). We also observed a general disorganization of the synaptic zones, with more synapses distributed relatively farther from the basal pole of the hair cell (Fig. 8, *B*, *D*, *F*), as noted in reference to the representative confocal images reproduced in Fig. 2 (*A* vs. *B*).

## DISCUSSION

*Effects of noise on low- vs. high-SR fiber neurophysiology.* The observations that AN fibers differ in threshold sensitivity, and that threshold is closely correlated with SR, were first described in cat (Liberman 1978), but the same relations have since been described in guinea pig (Tsuji and Liberman 1997), gerbil (Schmiedt 1989), mouse (Taberner and Liberman 2005), and rabbit (Borg et al. 1988), suggesting the low- vs. high-SR distinction represents a general mammalian plan for the auditory periphery. In cat and guinea pig, the distributions of spontaneous rate are fundamentally bimodal, suggesting that there are (at least) two very different groups of fibers rather than a continuum (Liberman and Kiang 1978; Tsuji and Liberman 1997).

The striking differences in central projections of low- vs. high-SR fibers (Liberman 1991) reinforce the notion that these neuronal groups play different roles in auditory processing. Clearly, connecting the sensory cells to the brain via fibers with a range of sensitivities must be important in extending the dynamic range of the auditory periphery. Perhaps more importantly, low-SR fibers, by virtue of their higher thresholds, are more resistant to masking by continuous background noise (Costalupes et al. 1984). Thus, to a certain extent, we must hear with our high-SR fibers in quiet backgrounds, but rely increasingly on the low-SR population as background noise increases. It has also been suggested that low-SR fibers are particularly important in driving the sound-driven reflexes to the auditory periphery, the middle-ear muscle reflex, and the medial olivocochlear bundle (Liberman 1988).

Suggestions that low-SR fibers are more vulnerable to cochlear insult have appeared in prior neurophysiological studies of acoustic trauma (Liberman 1978) and aging (Schmiedt et al. 1996). In an early study of alterations in AN response associated with noise-induced cochlear damage (Liberman 1978), some exposed ears showed a relative paucity of low-SR units, and a later study of aging gerbils (Schmiedt et al. 1996) noted a reduction in the proportion of low-SR fibers among AN fibers sampled. However, in both studies, there was a general elevation of cochlear thresholds: thus the lack of low-SR fibers could have arisen not because they had disappeared, but because they were bypassed when their thresholds rose above the level of the search stimulus used to identify neuronal contact when advancing the electrode.

Prior study in both mouse (Kujawa and Liberman 2009) and guinea pig (Lin et al. 2011) has shown that acoustic overexposures causing significant, but ultimately reversible, cochlear

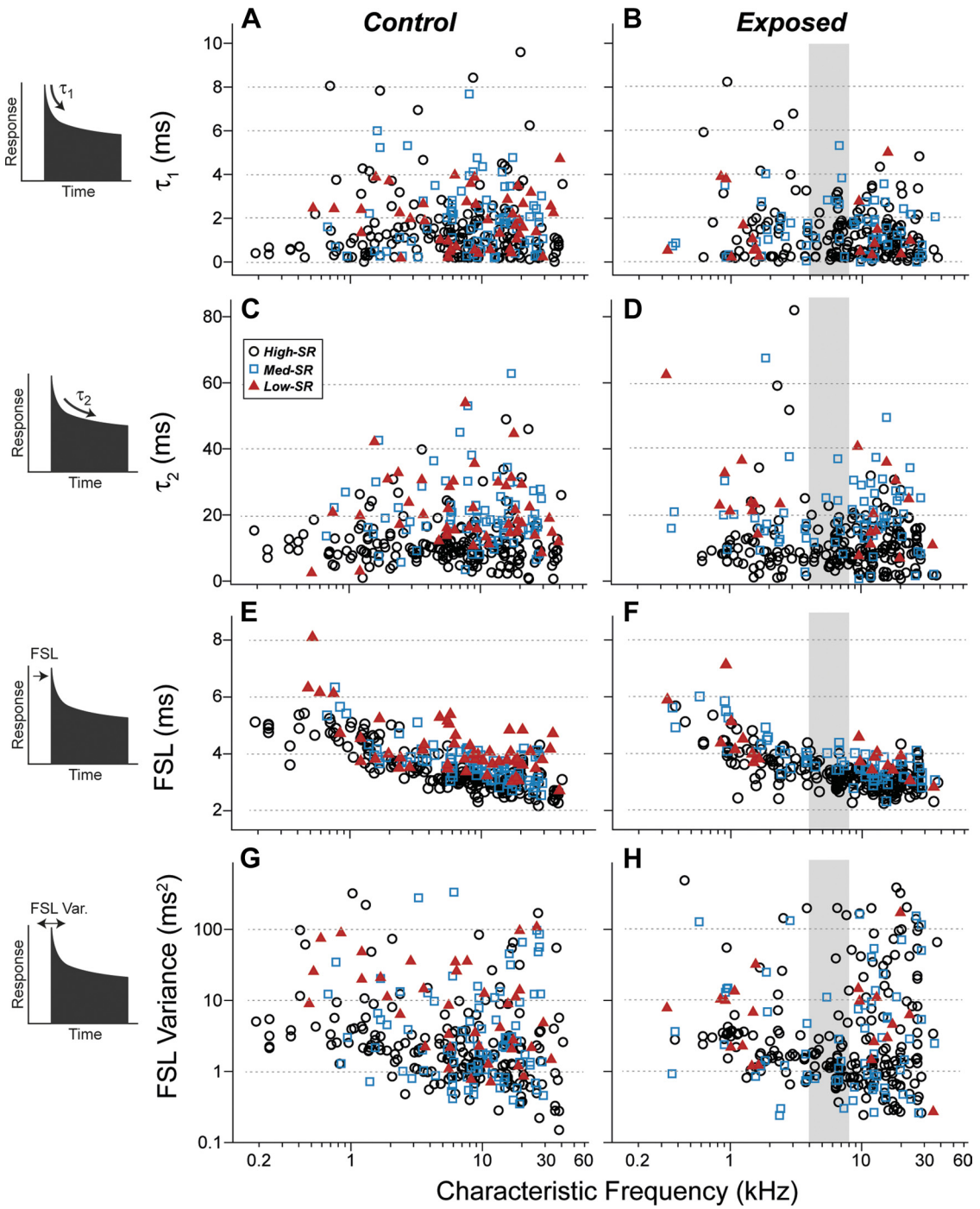


Fig. 7. Response dynamics in surviving cochlear nerve fibers were unchanged by the noise exposure. Poststimulus time histograms with a 0.1-ms bin width were computed for each fiber in response to CF tone bursts at 30 dB above threshold. From such histograms (schematized at *left*), several metrics were extracted from control fibers (*A*, *C*, *E*, *G*) and exposed fibers (*B*, *D*, *F*, *H*). *A–D*: the fast and slow time constants (t1 and t2) of postonset adaptation are defined by the double exponential function that provides the best fit to the first 85 ms of poststimulus time. *E–H*: first-spike latency (FSL) is the mode of the distribution of first-spike times in response to each tone burst. FSL variance is computed from the same distribution. Key in *C* applies to all panels.

threshold elevations can lead to significant loss of cochlear nerve fibers. This neural degeneration is seen first, i.e., within 24 h, as a loss of synapses on the IHCs throughout the basal half of the cochlea, and much more slowly, i.e., in months to years, as a loss of spiral ganglion cells and their central projections (Kujawa and Liberman 2009; Lin et al. 2011). The similarity of postexposure thresholds in DPOAEs and ABRs suggested that temporary threshold shifts are due predominately to reversible damage to the cochlear amplifier, i.e., the outer hair cells. Indeed, full recovery of hair cells was confirmed histologically. Two observations suggested that noise-induced primary neural degeneration might be selective for low-SR fibers: *1*) the neuronal loss was roughly 40%, which is comparable to the proportion of low-SR fibers in an unbiased sample of cochlear neurons (Liberman 1978; Tsuji and Liberman 1997), and *2*) a selective loss of high-threshold fibers

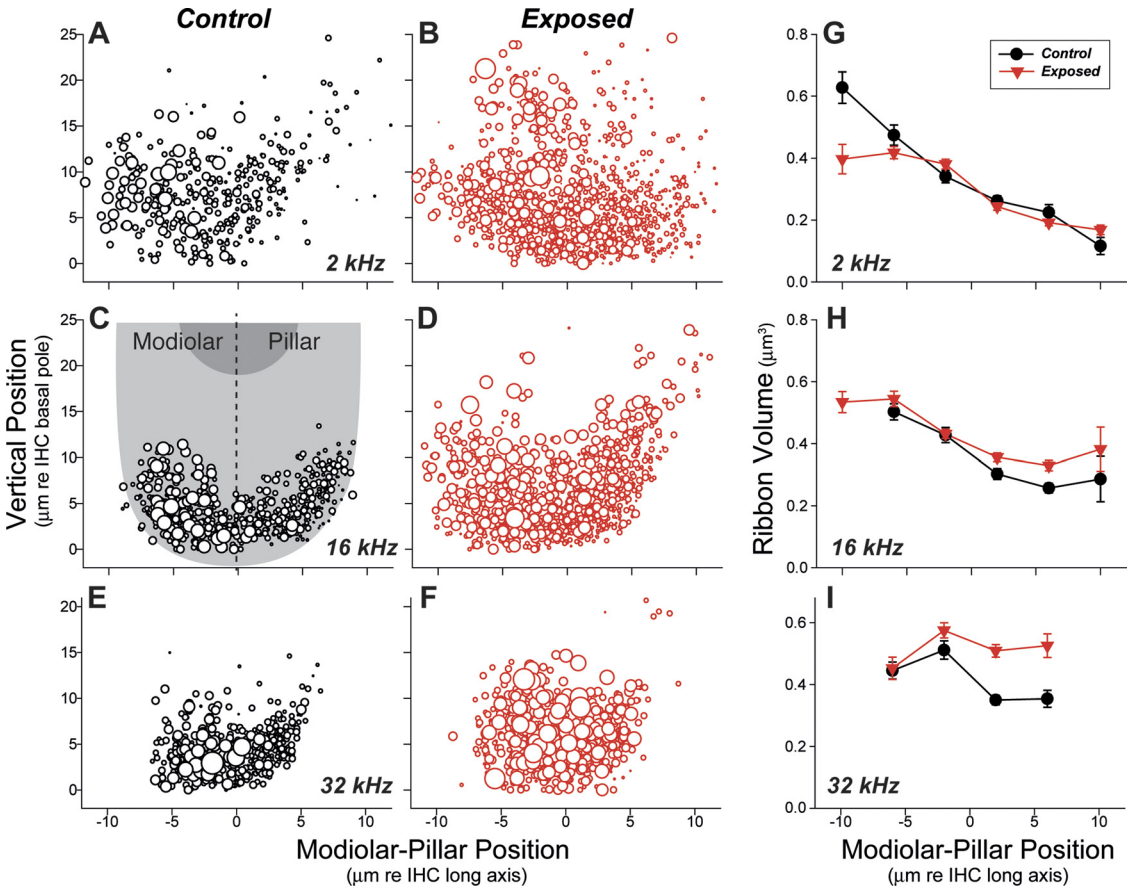


Fig. 8. Synaptic-ribbon volume is increased, and the normal modiolar-pillar ribbon gradient is disrupted, in noise-damaged cochlear regions. *A–F*: bubble plots compare the location and volumes of synaptic ribbons, in control vs. exposed ears, around the IHC basolateral membrane in 3 frequency regions: *A* and *B*, 2 kHz; *C* and *D*, 16 kHz; and *E* and *F*, 32 kHz. Volume is represented by symbol size, which is proportional to the silhouette area of each ribbon, if its measured volume were a perfect sphere. Vertical position and modiolar-pillar position are derived by transforming the coordinates of each z-stack, as schematized in *C*, such that the *y*-axis is parallel to the IHC long axis and bisects the IHC width. *G–I*: plots of mean ribbon volume (± SE) computed by dividing the same data shown in *A–F* into 4-$\mu$m bins of modiolar-pillar position. At each region, data from 2 control and 6 exposed ears are superimposed. Key in *G* also applies to *H* and *I*. Bins with fewer than 5 data points are not plotted.

would provide a natural explanation for the full recovery of ABR thresholds and the persistence of suprathreshold amplitude decreases.

The present results (Fig. 5) provide strong support for the idea that noise-induced synaptopathy is selective for the low-SR fiber group. However, given the nature of the experimental approach, it is impossible to rule out the possibility that SR of individual fibers is changed by the acoustic overexposure. Indeed, studies of acoustic trauma that produce permanent noise-induced threshold shifts have suggested that IHC stereocilia loss, which commonly underlies these irreversible changes, reduces the SR of all fibers, presumably because the loss of transduction channels decreases the resting current through the hair bundles, which in turn slightly hyperpolarizes the IHC and decreases spontaneous vesicle release (Liberman and Dodds 1984). In the presence of stereocilia damage, ANF SRs are never greater than ~40 sp/s (Liberman and Dodds 1984), rather than the 150 sp/s maximum seen in the present study. Thus, the simplest interpretation of the data in Fig. 5 is that SRs of the surviving fibers are unchanged.

Regardless of whether this simple interpretation is correct, the present study also shows that the noise exposure has caused a loss of fibers with high thresholds and large dynamic ranges (Figs. 4 and 6*B*). Regardless of what their preexposure SR was, this loss should decrease the information content in the auditory nerve, particularly in the presence of continuous background noise. This partial deafferentation may also be an important contributor to the generation of hyperactivity in the central auditory pathways that is commonly seen after acoustic overstimulation (e.g., Mulders et al. 2011). This, in turn, may be one source of tinnitus, the phantom auditory percept that is commonly associated with acoustic overexposure (Schmuzigert et al. 2006). Indeed, recent human studies have reported reductions in ABR wave 1 amplitude in tinnitus vs. non-tinnitus subjects with matching (normal) audiometric thresholds (Gu et al. 2012; Schaette and McAlpine 2011).

*Effects of noise on low- vs. high-SR fiber morphology.* Prior studies of the normal cochlea, at the light- and electron-microscopic level and in both cat and guinea pig, have shown that, although both low- and high-SR fibers contact a single IHC via a single terminal bouton, low-SR terminals tend to be smaller in caliber and their synapses are usually found on the modiolar-facing side of the IHC basolateral membrane (Liberman 1982b; Tsuji and Liberman 1997). An ultrastructural study of labeled, physiologically identified, ANFs in cat revealed the additional counterintuitive fact that low-SR synapses are characterized by exceptionally large, and often multiple, presynaptic ribbons, whereas high-SR ribbons are small

singlets (Merchan-Perez and Liberman 1996). A subsequent light-microscopic confocal study in mouse confirmed the ribbon size gradient (larger ribbons on the modiolar side) and suggested that an opposing gradient of glutamate receptor-patch size (smaller patches on the modiolar side) could contribute to the differences in neuronal sensitivity (Liberman et al. 2011). The present study confirms the ribbon size gradient in the normal guinea pig ear (Fig. 8); however, a clear-cut glutamate patch gradient was not observed. The significance of this discrepancy is not clear.

Prior studies of noise-induced neuropathy in the mouse and guinea pig relied mainly on counts of presynaptic ribbons to assess the changes in afferent innervation in the IHC area (Kujawa and Liberman 2009; Lin et al. 2011). However, in the guinea pig study, quantification of AN terminals was attempted by immunostaining for neurofilament and assessing the apposition of ribbons and terminals. In the normal ear, 20% of ribbons were not opposed by terminals, and in the noise-exposed ear that percentage rose to ~40% (Lin et al. 2011). In the present study, using glutamate-receptor immunostaining to assess the postsynaptic elements, we saw a similar trend, i.e., that the numbers of orphan (unpaired) ribbons rises after noise exposure; however, the absolute numbers were 10× lower: i.e., 2% in control ears rising to ~4% in exposed ears (Fig. 3). This discrepancy likely arises because neurofilaments do not always invade the terminal bouton, thus the apposition between pre- and postsynaptic immunostaining is not as reliably close as that seen with the glutamate receptor label. Serial section ultrastructural work shows that orphan ribbons are indeed very rare in the normal ear (Liberman 1980; Stamataki et al. 2006), thus we believe that the present results (showing 98% of normal ribbons paired with postsynaptic terminals) are more accurate than those seen with neurofilament immunostaining, which will overestimate the number of orphan ribbons. The relatively small number of orphan ribbons, even after noise exposure, further suggests that ribbon counts are a very good proxy for synaptic counts in this model system.

The synaptic changes observed in the present study were not those predicted from simply eliminating the low-SR elements (i.e., large ribbons on the modiolar side) from the normal synaptic architecture. Rather, there was an increase in mean ribbon size, these abnormally large ribbons were found on both sides of the IHC, and there was no obvious decrease in the proportion of modiolar vs. pillar ribbons (Fig. 8). These observations suggest that ribbon size is plastic and that synapses may redistribute around the IHC circumference after the disappearance of a (putatively low-SR) subset of the afferent terminals. They also suggest that the normal inverse correlation between ribbon size and SR is not causal, since a postexposure increase in ribbon size was seen here despite a postexposure increase in mean spontaneous rate. The dramatic morphological changes in the remaining ribbons are noteworthy given the lack of physiological changes in the surviving postsynaptic neurons. However, this is perhaps not surprising given the normality of many aspects of AN response in mutant mice with complete absence of presynaptic ribbons in the IHCs (Buran et al. 2010).

*Excitotoxicity and the special vulnerability of low-SR fibers.* Numerous prior studies have noted that acoustic overstimulation causes dramatic swelling of the ANF terminals in the IHC area, if the ear is fixed with 24- to 48-h postexposure (Liberman and Mulroy 1982; Robertson 1983). Similar swelling of terminals can be seen after perfusing the cochlea with glutamate agonists, and the appearance of noise-induced swelling can be partially blocked by perfusing the cochlea with glutamate antagonists (Pujol et al. 1993). Neither the noise-induced, nor the kainate-induced, terminal swelling is seen in the terminals of type II fibers contacting outer hair cells. Together, these observations have suggested that the phenomenon is a type of glutamate excitotoxicity and that the pathology is restricted to the IHC area because the type II terminals do not express the same AMPA type glutamate receptors (e.g., GluA2) as do the type I terminals (Liberman et al. 2011).

The present results suggest that the low-SR fibers are more vulnerable to this putative glutamate excitotoxicity. Despite their lower thresholds to acoustic stimulation, spike rate in high-SR AN fibers tends to saturate within 30 dB of threshold (Winter et al. 1990); thus, the steady-state discharge rate in response to the traumatic noise band at 106 dB SPL will likely be the same, or less, in low- vs. high-SR fibers. The heightened vulnerability of low-SR fibers could arise in a number of ways. It is possible, for example, that the clearance of released glutamate is less effective on the modiolar, than on the pillar, side of the IHC; indeed, immunostaining for the GLAST transporter, which clears glutamate from the synaptic cleft into the IHC's supporting cells, is less intense on the low-SR (modiolar) side of the IHC (Furness and Lawton 2003). Another hypothesis is that the differences arise from the fact that low-SR fibers contain many fewer mitochondria than high-SR fibers, a difference that presumably reflects the increased demand on $Na^+/K^+$ pumping in those neurons that are discharging at rates of up to 100 sp/s even in complete quiet (Liberman 1980). Studies of glutamate excitotoxicity in central neurons suggest that $Ca^{2+}$ entry is an important upstream event in the excitotoxicity cascade, and that mitochondria are a crucial source of Ca buffering capacity (Szydlowska and Tymianski 2010).

If low-SR fibers are indeed less well equipped to deal with steady glutamate release during a 2-h acoustic overexposure such as in the present study, it is possible that they are also more vulnerable to repeated stimulation at much lower SPLs, i.e., those presented in the course of everyday acoustic environments, and, thus, that the normal process of aging may also be characterized by a type of low-SR neuropathy. Given the view that low-SR fibers may be particularly important to hearing in a noisy environment, a selective and progressive low-SR neuropathy may be an important contributor to the increasing hearing impairments that characterize the aging human population.

**ACKNOWLEDGMENTS**

The skillful assistance of Leslie Dodds in cochlear immunochemistry is gratefully acknowledged.

**GRANTS**

This work was supported by research, core, and training grants from National Institute on Deafness and Other Communication Disorders RO1 DC-00188 (M. C. Liberman), P30 DC-05029 (M. C. Liberman), R01 DC-08577 (S. G. Kujawa), and T32 DC-00038 (A. C. Furman).

**DISCLOSURES**

No conflicts of interest, financial or otherwise, are declared by the author(s).

## AUTHOR CONTRIBUTIONS

A.C.F., S.G.K., and M.C.L. conception and design of research; A.C.F. performed experiments; A.C.F., S.G.K., and M.C.L. analyzed data; A.C.F., S.G.K., and M.C.L. interpreted results of experiments; A.C.F. and M.C.L. prepared figures; A.C.F. and M.C.L. drafted manuscript; A.C.F., S.G.K., and M.C.L. edited and revised manuscript; A.C.F., S.G.K., and M.C.L. approved final version of manuscript.

## REFERENCES


**Bohne BA, Kenworthy A, Carr CD.** Density of myelinated nerve fibers in the chinchilla cochlea. *J Acoust Soc Am* 72: 102–107, 1982.

**Borg E, Engstrom B, Linde G, Marklund K.** Eighth nerve fiber firing features in normal-hearing rabbits. *Hear Res* 36: 191–202, 1988.

**Buran BN, Strenzke N, Neef A, Gundelfinger ED, Moser T, Liberman MC.** Onset coding is degraded in auditory nerve fibers from mutant mice lacking synaptic ribbons. *J Neurosci* 30: 7587–7597, 2010.

**Cheatham MA, Huynh KH, Gao J, Zuo J, Dallos P.** Cochlear function in Prestin knockout mice. *J Physiol* 560: 821–830, 2004.

**Costalupes JA, Young ED, Gibson DJ.** Effects of continuous noise backgrounds on rate response of auditory nerve fibers in cat. *J Neurophysiol* 51: 1326–1344, 1984.

**Furness DN, Lawton DM.** Comparative distribution of glutamate transporters and receptors in relation to afferent innervation density in the mammalian cochlea. *J Neurosci* 23: 11296–11304, 2003.

**Gu JW, Herrmann BS, Levine RA, Melcher JR.** Brainstem auditory evoked potentials suggest a role for the ventral cochlear nucleus in tinnitus. *J Assoc Res Otolaryngol* 13: 819–833, 2012.

**Kiang NY, Watanabe T, Thomas EC, Clark LF.** *Discharge patterns of single fibers in the cat's auditory nerve.* Cambridge, MA: MIT Press, 1965, p. 154.

**Kujawa SG, Liberman MC.** Adding insult to injury: cochlear nerve degeneration after "temporary" noise-induced hearing loss. *J Neurosci* 29: 14077–14085, 2009.

**Liberman LD, Wang H, Liberman MC.** *Opposing gradients of ribbon size and AMPA receptor expression underlie sensitivity differences among cochlear-nerve/hair-cell synapses.* J Neurosci 31: 801–808, 2011.

**Liberman MC.** Auditory-nerve response from cats raised in a low-noise chamber. *J Acoust Soc Am* 63: 442–455, 1978.

**Liberman MC.** Central projections of auditory nerve fibers of differing spontaneous rate. I. Anteroventral cochlear nucleus. *J Comp Neurol* 313: 240–258, 1991.

**Liberman MC.** The cochlear frequency map for the cat: labeling auditory-nerve fibers of known characteristic frequency. *J Acoust Soc Am* 72: 1441–1449, 1982a.

**Liberman MC.** Morphological differences among radial afferent fibers in the cat cochlea: an electron-microscopic study of serial sections. *Hear Res* 3: 45–63, 1980.

**Liberman MC.** Physiology of cochlear efferent and afferent neurons: direct comparisons in the same animal. *Hear Res* 34: 179–192, 1988.

**Liberman MC.** Single-neuron labeling in the cat auditory nerve. *Science* 216: 1239–1241, 1982b.

**Liberman MC, Dodds LW.** Single-neuron labeling and chronic cochlear pathology. II. Stereocilia damage and alterations of spontaneous discharge rates. *Hear Res* 16: 43–53, 1984.

**Liberman MC, Dodds LW, Pierce S.** Afferent and efferent innervation of the cat cochlea: quantitative analysis with light and electron microscopy. *J Comp Neurol* 301: 443–460, 1990.

**Liberman MC, Kiang NY.** Acoustic trauma in cats. Cochlear pathology and auditory-nerve activity. *Acta Otolaryngol* 358: 1–63, 1978.

**Liberman MC, Mulroy MJ.** Acute and chronic effects of acoustic trauma: cochlear pathology and auditory nerve pathophysiology. In: *New Perspectives on Noise-Induced Hearing Loss*, edited by Hamernik RP, Henderson D, and Salvi R. New York: Raven Press, 1982, p. 105–136.

**Lin HW, Furman AC, Kujawa SG, Liberman MC.** Primary neural degeneration in the Guinea pig cochlea after reversible noise-induced threshold shift. *J Assoc Res Otolaryngol* 12: 605–616, 2011.

**Melcher JR, Knudson IM, Fullerton BC, Guinan JJ Jr, Norris BE, Kiang NY.** Generators of the brainstem auditory evoked potential in cat. I. An experimental approach to their identification. *Hear Res* 93: 1–27, 1996.

**Merchan-Perez A, Liberman MC.** Ultrastructural differences among afferent synapses on cochlear hair cells: correlations with spontaneous discharge rate. *J Comp Neurol* 371: 208–221, 1996.

**Mulders WH, Ding D, Salvi R, Robertson D.** Relationship between auditory thresholds, central spontaneous activity, and hair cell loss after acoustic trauma. *J Comp Neurol* 519: 2637–2647, 2011.

**Neef A, Khimich D, Pirih P, Riedel D, Wolf F, Moser T.** Probing the mechanism of exocytosis at the hair cell ribbon synapse. *J Neurosci* 27: 12933–12944, 2007.

**Pujol R, Puel JL, Gervais d'Aldin C, Eybalin M.** Pathophysiology of the glutamatergic synapses in the cochlea. *Acta Otolaryngol* 113: 330–334, 1993.

**Robertson D.** Functional significance of dendritic swelling after loud sounds in the guinea pig cochlea. *Hear Res* 9: 263–278, 1983.

**Schaette R, McAlpine D.** Tinnitus with a normal audiogram: physiological evidence for hidden hearing loss and computational model. *J Neurosci* 31: 13452–13457, 2011.

**Schmiedt RA.** Spontaneous rates, thresholds and tuning of auditory-nerve fibers in the gerbil: comparisons to cat data. *Hear Res* 42: 23–36, 1989.

**Schmiedt RA, Mills JH, Boettcher FA.** Age-related loss of activity of auditory-nerve fibers. *J Neurophysiol* 76: 2799–2803, 1996.

**Schmuzigert N, Fostiropoulos K, Probst R.** Long-term assessment of auditory changes resulting from a single noise exposure associated with non-occupational activities. *Int J Audiol* 45: 46–54, 2006.

**Spoendlin H.** Innervation patterns in the organ of corti of the cat. *Acta Otolaryngol* 67: 239–254, 1969.

**Stamataki S, Francis HW, Lehar M, May BJ, Ryugo DK.** Synaptic alterations at inner hair cells precede spiral ganglion cell loss in aging C57BL/6J mice. *Hear Res* 221: 104–118, 2006.

**Szydlowska K, Tymianski M.** Calcium, ischemia and excitotoxicity. *Cell Calcium* 47: 122–129, 2010.

**Taberner AM, Liberman MC.** Response properties of single auditory nerve fibers in the mouse. *J Neurophysiol* 93: 557–569, 2005.

**Tsuji J, Liberman MC.** Intracellular labeling of auditory nerve fibers in guinea pig: central and peripheral projections. *J Comp Neurol* 381: 188–202, 1997.

**Westerman LA, Smith RL.** Rapid and short-term adaptation in auditory nerve responses. *Hear Res* 15: 249–260, 1984.

**Winter IM, Robertson D, Yates GK.** Diversity of characteristic frequency rate-intensity functions in guinea pig auditory nerve fibres. *Hear Res* 45: 191–202, 1990.